Developmental Biology 330 (2009) 427–439

Contents lists available at ScienceDirect

Developmental Biology

journal homepage: www.elsevier.com/developmentalbiology

Evidence for crucial role of hindgut expansion in directing proper migration of primordial germ cells in mouse early embryogenesis

Kenshiro Hara [a], Masami Kanai-Azuma [b], Mami Uemura [a], Hiroshi Shitara [c], Choji Taya [c], Hiromichi Yonekawa [c], Hayato Kawakami [b], Naoki Tsunekawa [a], Masamichi Kurohmaru [a], Yoshiakira Kanai [a,*]

[a] Department of Veterinary Anatomy, The University of Tokyo, Yayoi 1-1-1, Bunkyo-ku, Tokyo 113-8657, Japan
[b] Department of Anatomy, Kyorin University School of Medicine, Mitaka, Tokyo 181-8611, Japan
[c] The Tokyo Metropolitan Institute of Medical Science, 3-18-22, Bunkyo-ku, Tokyo 113-8613, Japan

ARTICLE INFO

Article history:
Received for publication 10 February 2009
Revised 18 March 2009
Accepted 7 April 2009
Available online 14 April 2009

Keywords:
Primordial germ cells
Migration
Sox17
Hindgut endoderm
Chimera
Mice

ABSTRACT

During mouse gastrulation, primordial germ cells (PGCs) become clustered at the base of the allantois and move caudally into the hindgut endoderm before entering the genital ridges. The precise roles of endoderm tissues in PGC migration, however, remain unclear. By using *Sox17* mutants with a specific endoderm deficiency, we provide direct evidence for the crucial role of hindgut expansion in directing proper PGC migration. In *Sox17*-null embryos, PGCs normally colonize in the allantois and then a small front-row population of PGCs moves properly into the most posterior gut endoderm. Defective hindgut expansion, however, causes the failure of further lateral PGC movement, resulting in the immobilization of PGCs in the hindgut entrance at the later stages. In contrast, the majority of the remaining PGCs moves into the visceral endoderm layer, but relocate outside of the embryonic gut domain. This leads to a scattering of PGCs in the extraembryonic yolk sac endoderm. This aberrant migration of *Sox17*-null PGCs can be rescued by the supply of wildtype hindgut cells in chimeric embryos. Therefore, these data indicate that hindgut morphogenic movement is crucial for directing PGC movement toward the embryonic gut side, but not for their relocation from the mesoderm into the endoderm.

Introduction

In developing mouse embryos, PGCs arise from a pluripotent population of cells in the proximal epiblast at around 6.25 days post coitum (dpc), and then move to and aggregate in the extraembryonic mesoderm at the base of the allantois by 7.25 dpc (Ohinata et al., 2005; McLaren and Lawson, 2005). Thereafter, most PGCs move caudally from the extraembryonic mesoderm position into the hindgut endoderm at approximately 7.5 to 8.5 dpc. Then, PGCs migrate to the mesentery of the hindgut from around 9.0 dpc, colonizing the genital ridges from 9.5 to 10.5 dpc. Recent studies indicate the presence of a highly conserved mechanism for PGC guidance into the gonads by chemokine SDF-1 (Doitsidou et al., 2002; Ara et al., 2003; Knaut et al., 2003; Molyneaux et al., 2003; Stebler et al., 2004; Boldajipour et al., 2008; Herpin et al., 2008; Sasado et al., 2008). In mouse embryogenesis, the activities of both SDF-1 and its receptor CXCR4 are crucial for proper PGC movement from the hindgut walls into the genital ridges from 9.5 to 10.5 dpc (*SDF-1*-null embryos: Ara et al., 2003; *CXCR4*-null embryos: Molyneaux et al., 2003). At early migratory stages before 9.0 dpc, however, neither SDF-1 nor CXCR4 is essential for PGC migration to the hindgut endoderm. In zebrafish, however, SDF-1/CXCR4 signaling appears to completely guide the migratory path of PGCs into the gonads from their specification sites (Doitsidou et al., 2002; Knaut et al., 2003). Tanaka et al. (2005), on the other hand, recently proposed a unique model of "homing and repulsion" mediated by *Ifitm* genes in PGCs and mesoderm, claiming that *Ifitm1* activity in the mesoderm acts as a repulsion guidance cue for *Ifitm3*-positive and *Ifitm1*-negative PGCs into the *Ifitm*-free endoderm. However, recent genetic analysis by targeted disruption of the entire *Ifitm* locus clearly showed no detectable influences on migration and development of the germ cell line in mouse embryos lacking all *Ifitm* genes (Lange et al., 2008), suggesting that *Ifitm* genes play a minor role in the guidance of PGC migration from the allantois into the hindgut endoderm. Therefore, the molecular and cellular mechanisms involved in PGC migration into the hindgut endoderm in mouse embryogenesis remain unclear.

The PGC migration route via endodermal tissues is widely conserved in several vertebrate and invertebrate species (i.e., gut precursor (E) cells in *C. elegans* (Sulston et al., 1983); midgut in *Drosophila* [Warrior, 1994]; endoderm in frogs (Whitington and Dixon, 1975; Subtelny and Penkala, 1984; Nishiumi et al., 2005), and

* Corresponding author. Fax: +81 3 5841 8181.
E-mail address: aykanai@mail.ecc.u-tokyo.ac.jp (Y. Kanai).

0012-1606/$ – see front matter © 2009 Elsevier Inc. All rights reserved.
doi:10.1016/j.ydbio.2009.04.012

hindgut in mice [Molyneaux and Wylie, 2004]), suggesting a potential link of endoderm development and PGC migration and differentiation during early migratory stages. It has also been shown that, during PGC movement within hindgut endoderm, PGCs initiate a genome-wide demethylation (Seki et al., 2005, 2007; see in review Sasaki and Matsui, 2008) and X reactivation (de Napoles et al., 2007; Sugimoto and Abe, 2007) as well as alterations in gene expression (Nakamuta and Kobayashi, 2004; Kurimoto et al., 2008). At similar stages, PGCs undergo a significant reduction in dimethylated histone H3 lysine9 (diMeH3K9), a repressive modification of their genome, and instead acquire high levels of trimethylated histone H3K27 (triMeH3K27) at around 8.5 dpc (Seki et al. 2005, 2007). Such dynamic epigenetic alterations and histone modifications at these hindgut stages clearly suggest a possible supportive function of hindgut endoderm in PGC differentiation. Moreover, several previous morphological studies have revealed non-motile behavior of PGCs at the early hindgut stage, characterized by round cells without pseudopodial projections (Clark and Eddy, 1975; Anderson et al., 2000). These previous studies clearly suggest that the morphogenic movement of hindgut endoderm itself may be one of the major factors directing PGCs to the proper migratory path into the genital ridges. However, there is still no direct evidence whether the movement of PGCs from the allantois into the hindgut is an active migration or part of a morphogenic tissue movement.

It is now well-established that *Sox17* is crucial for definitive endoderm formation in various vertebrates (Hudson et al., 1997; Alexander and Stainier, 1999; Tam et al., 2003). Our previous study showed that *Sox17* is highly activated in endodermal tissues during early gastrulation, and that its activity is specifically required for gut endoderm expansion (Kanai-Azuma et al., 2002; this study). Since *Sox17*-null embryos display failed hindgut expansion without any appreciable defects in other tissues by early-somite stages (Kanai-Azuma et al., 2002), this mutant embryo is a useful mouse model for studies on the potential inductive and supportive functions of hindgut endoderm in mouse early embryogenesis.

In order to clarify the endodermal role in PGC migration and differentiation, the present study examined the influence of defective development of the hindgut endoderm for PGC migration and differentiation using *Sox17*-null embryos mixed with or without wildtype endoderm cells. Our study provides direct genetic evidence that hindgut endoderm expansion is essential for directing the localization of PGC in the embryonic gut, not for specification or differentiation until early-somite stages. Finally, we suggested the importance of the synchronized movement of hindgut endodermal cells and PGCs at the hindgut entrance for proper PGC migration to genital ridges based on our observation that most PGCs migrated ectopically into the yolk sac visceral endoderm.

Materials and methods

Animals and chimeric embryos

Embryos at 7.5 to 9.0 dpc were obtained from pregnant wildtype (ICR strain) and *Sox17* heterozygous female mice mated with *Sox17* heterozygous male mice (ICR background). Chimeric embryos with *Sox17*-null mutant ES cells at 8.75 to 9.0 dpc were also generated by blastocyst injection of *Sox17*-null ES cells into C57BL/6-Tg (CAG-EGFP) mice (Green mice; Japan SLC, Inc.) as described previously (Kanai-Azuma et al., 2002). Genomic DNA from the tail tip of mice was isolated using a Wizard® Genomic DNA Purification Kit (Promega). For embryo DNA, part of the anterior extraembryonic region was dissected from each embryo, and genomic DNA was prepared using the same kit as for PCR analysis of embryonic genotype, as described previously (Kanai-Azuma et al., 2002). All animal experiments were conducted in accordance with the Guidelines for Animal Use and Experimentation as set out by the University of Tokyo.

Standard alkaline phosphatase (ALP) staining and count of ALP-positive PGC number

To count the number of ALP-positive PGCs in each *Sox17*-mutant or wildtype embryo, embryos before the stage of 5 to 6 somites were left intact, and then the anterior extra- and intraembryonic portions were split to expose the posterior allantois mesoderm and primitive streak tissues. After 7-somite stage, the posterior portions of the embryos were dissected, and split longitudinally along the line of the dorsal aorta to expose the hindgut area. All samples were fixed in 4% PFA-PBS for 6 h at 4 °C, and washed in TBST for 12 h. For permeabilization, the specimens were thoroughly dehydrated and then stored in 70% ethanol at 4 °C for more than 3 days. Finally, after washing with ALP buffer (100 mM Tris HCl (pH 9.5), 50 mM $MgCl_2$, 100 mM NaCl, 0.1% Tween-20), the specimens were stained with BCIP-NBT (Roche) in ALP buffer at 4 °C. The stained embryos were incubated with 70% glycerol to obtain optically clear tissue, and then flattened by a cover glass. The numbers of ALP-positive PGCs in the gut endoderm, extraembryonic visceral endoderm and allantois regions of wildtype, *Sox17*-heterozygote and *Sox17*-null embryos were counted separately using a compound microscope.

Whole-mount ALP staining without permeabilization and horseradish peroxidase (HRP) labeling for visualization of the visceral endoderm

Embryos were dissected at 7.75 to 8.25 dpc and incubated in Dulbecco's Modified Eagle's Medium (DMEM) containing BSA (2.5 mg/ml) and horseradish peroxidase (HRP; Sigma type IV, 1 mg/ml) for 30 min as described previously (Kanai-Azuma et al., 2002). The embryos were fixed in 4% PFA-PBS and then developed by DAB reaction. Next, the HRP-stained embryos were washed with ALP buffer and stained with BCIP-NBT (Roche) in ALP buffer at 4 °C without any permeabilization steps (i.e., dehydration by methanol and storage in 70% ethanol). After counting the number of ALP-positive PGCs on the surface of each embryo for accurate staging of late gastrulation at headfold stages, some samples were sagitally cryosectioned to confirm the ALP-positive signals detected in the only PGCs located in the outer endoderm layer.

DiI labeling and whole-embryo culture

The most posterior endoderm area of the embryos at 7.75 dpc was labeled with DiI (0.84 μg/μl, Invitrogen) using a micropipette (see Fig. 1G). After rinsing with DMEM, embryos were cultured for 12 h in DMEM supplemented with 75% rat serum using a rotating-bottle culture unit (Sturm and Tam, 1993). After the living embryos were photographed with a fluorescence microscope, they were fixed in 4% PFA-PBS and stained for whole-mount ALP activity as described above.

Immunohistochemistry

For whole-mount immunostaining, the embryos were fixed in 4% PFA-PBS for 6 h at 4 °C, and then washed with TBST. For permeabilization, all embryos were dehydrated and stored in 70% ethanol for several days. Then the embryos were incubated with anti-PGC7 antibody (1/10,000 dilution, kindly provided by Dr. Y. Matsui, Tohoku University, Japan) for 12 h at 4 °C. After washing with TBST, the signals were detected with Alexa-488/594 conjugated anti-rabbit IgG antibodies (1/200 dilution; Invitrogen).

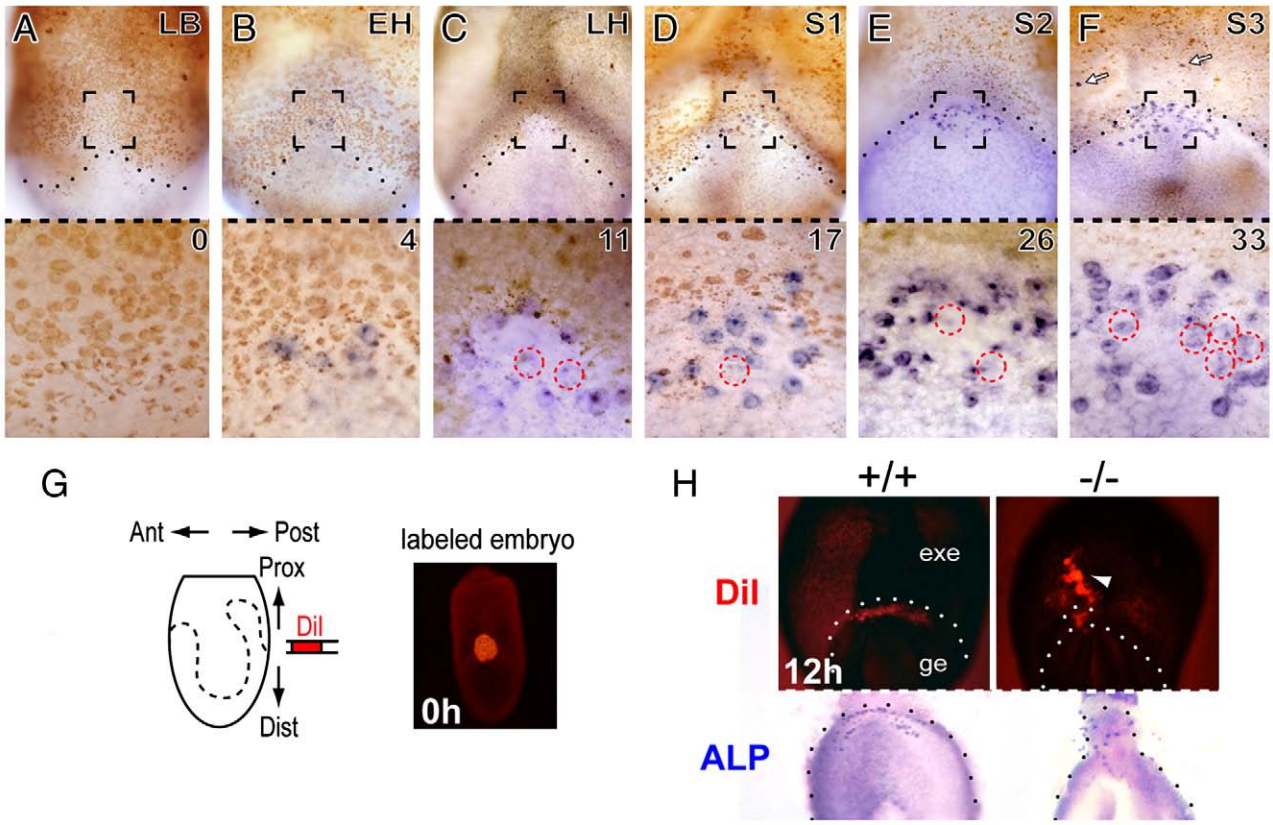

Fig. 1. Spatiotemporal migration patterns of PGCs and hindgut endoderm cells during late gastrulation and early somitogenesis. (A–F) Double-staining of wildtype embryos (ICR strain) at late-bud (A), early (B)- and late (C)-headfold, 1 (D)-, 2 (E)- and 3 (F)-somite stages (posterior view), showing HRP-positive visceral endoderm (brown staining) and ALP-positive germ cells (purple staining) located in the endoderm layer. Lower plates indicate higher magnified images surrounded by a broken rectangle in the upper plates. In each embryo, the number of PGCs which moved out into the endoderm layer is shown in the upper right corner of the lower panel. In lower plates, weak ALP-positive cells are seen in the PGC entry site (broken red circles). In F, open arrows indicate ectopic PGCs located in the extraembryonic yolk sac endoderm. (G, H) The most posterior gut endoderm area, including the PGC entry site (early-headfold stage; 7.75 dpc), were labeled with DiI (G) and then cultured for 12 h in a rotating-bottle culture unit (H). In G, left (lateral view) and right (posterior view) plates show schematic and fluorescence images of DiI-labeled embryos, respectively. (H) In wildtype (+/+) embryos, DiI-labeled endoderm cells (upper) and ALP-positive PGCs (lower) move into the lateral hindgut endoderm area (left in H), while neither shows any appreciable movement into the lateral gut area in *Sox17*-null embryos (right in H). Arrowhead indicates the movement of the DiI-labeled endoderm away from the gut domain. Small dots indicate the border between intra- (definitive) and extraembryonic (visceral) endoderm. exe, extraembryonic visceral endoderm; ge, gut endoderm.

For immunostaining of paraffin sections, the embryos were fixed in 4% PFA-PBS for 12 h at 4 °C, dehydrated, and then routinely embedded in paraffin. Deparaffinized sections were pre-stained for ALP activity using BCIP-NBT (purple staining) or a HNPP-Fluorescent Detection set (Roche). Then the sections were incubated with anti-diMeH3K9 (1/500 dilution; Upstate), anti-triMeH3K27 (1/500 dilution; Upstate), anti-5-methyl cytosine (MeC) (1/250 dilution; Calbiochem), anti-E-cadherin (1/500 dilution; BD-Pharmingen) or anti-p63 antibody (1/50 dilution; Santa Cruz). Finally, the immunoreaction was visualized by biotin-conjugated secondary Antibody in combination with an ABC Kit (Vector labs; brown staining) or by Alexa-488/594 conjugated secondary antibodies.

For immunostaining of frozen sections, chimeric embryos or ALP-pre-stained embryos were fixed in 4% PFA-PBS and then serially cryosectioned (8-12 μm in thickness). Every fourth frozen sections corresponding to the whole posterior trunk region were incubated with anti-PGC7 (1/10,000 dilution), anti-E-cadherin (1/500 dilution) or anti-laminin antibody (1/1000 dilution; ICN Pharmaceuticals). The signals were visualized by Alexa-488/594 conjugated secondary antibodies. In the chimeric and non-chimeric embryos, the genotype of each PGC/hindgut cell was estimated by EGFP signal intensity (wildtype: EGFP-positive versus *Sox17*-null: EGFP-negative cells), and then the cell numbers in all anti-PGC7-stained sections of embryos (total average 34.2 sections per embryo) were counted separately. In some sections stained with anti-PGC7 antibody, the signals were also stripped in 0.2 M glycine/0.1% Tween-20 (pH 2.2), and re-stained for anti-laminin immunostaining.

Multiple immunofluorescence images were visualized using pseudo-colored red, green, blue and white to display the distribution of up to four fluorescent signals.

In situ hybridization

Whole-mount *in situ* hybridization was performed as previously described by Kanai-Azuma et al. (1999). In short, the embryos were fixed in 4% PFA-PBS for 6 h, and then dehydrated in methanol. The samples were pretreated with proteinase K, and hybridized with DIG-labeled *Ifitm3* RNA probe (Tanaka and Matsui, 2002: kindly provided by Dr. S.S. Tanaka, Kumamoto University, Japan). After treatment with RNase, they were finally washed with 2× SSC/50% formamide for 1 h at 65 °C. The signals were detected by an immunological method using ALP-conjugated anti-DIG antibody.

Transmission electron microscopy

Isolated embryos were fixed in 2.5% glutaraldehyde/0.1 M phosphate buffer (PB) for 4 h at 4 °C. After washing with PBS, they were postfixed in 1% OsO_4 in 0.1 M PB for 2 h at 4 °C. They were then

dehydrated and embedded in Araldite M. Ultrathin sections were examined under a JEOL-1010 transmission electron microscope at 80 kV.

Statistical analysis

The number of PGCs in each genotype was analyzed quantitatively by Student's *t*-test and the nonparametric Mann–Whitney *U*-test. Difference of correlation coefficients of the linear regression lines was compared by testing the *t*-value.

Results

Spatiotemporal patterns of PGC movement into the outer endoderm layer at gastrulation stage

First, in order to confirm the timing and entry site of PGC movement from the allantois mesoderm into the outer endoderm layer, we isolated intact whole embryos at the late-bud to early-somite stages (7.5–8.25 dpc), incubated them with HRP (for the uptake activity of visceral endoderm; Bielinska et al., 1999), and then examined the specimens by whole-mount ALP/HRP double-staining without any permeabilization steps. This procedure enabled visualization of both HRP-labeled visceral endoderm (brown staining) and ALP-positive PGCs that are located within the gut endoderm (blue staining) at the most posterior gut region of the mouse embryos (Figs. 1A–F). Under these staining conditions, no ALP-positive reactions were detected in PGCs located within the allantois region (Fig. 1A). This finding was also confirmed histologically by frozen sectioning (figures not shown). As shown in Fig. 1, at around the headfold stage (7.75 dpc), a small front-row population of four to six PGCs was first detected in the PGC entry site located in the most posterior embryonic endoderm at the base of the allantois (broken rectangle in Fig. 1B). Thereafter, the ALP-positive PGC population appears to increase in number (Figs. 1C, D) before spreading into the lateral hindgut region just near the extraembryonic area (Figs. 1E, F). Coincidental with the lateral movement of PGCs (roughly when approximately 15–18 PGCs appear in the surface endoderm region), the HRP-negative embryonic endoderm area expanded into the lateral hindgut area (dots in Figs. 1D–F). In contrast, a very weak ALP-positive population of PGCs persisted in the central area of the PGC entry site (broken red circles in lower Figs. 1C–F). Analyses of the sectioning samples and planar samples of the posterior embryonic parts (pressed by cover glass) also confirmed that these weak ALP-positive PGCs were located immediately beneath, or near, the hindgut endoderm area (Supplementary information, Fig. S1), suggesting that the PGC entry site is a restricted central area in the most posterior endoderm region. Only a small population of PGCs ($3.0+/-1.8$ per embryo; $n=30$ embryos at 3–5 somite stages) was located in the HRP-positive visceral endoderm area (open arrows in Fig. 1F). Most ALP-positive PGCs were detected inside the HRP-negative embryonic endoderm region at early-somite stages. Finally, all PGCs (approximately 30–35) migrated into the outer hindgut endoderm layer by the 3–4 somite stage.

Sox17-null embryos display defective expansion of the hindgut endoderm population corresponding to the PGC entry site at late gastrulation stage

In order to examine the morphogenic movement of hindgut endoderm cells using fluorescent dye DiI, we labeled the endoderm area including the PGC entry site in wildtype and *Sox17*-null embryos at early-headfold stage (Fig. 1G), and then cultured them for 12 h. As shown in Fig. 1H, both DiI-labeled endoderm cells and PGCs moved properly into the lateral gut area in wildtype embryos. This finding is consistent with the previous data obtained by Tanaka et al. (2005). In *Sox17*-null embryos, on the other hand, DiI-labeled endoderm cells were defective in their movement into the lateral gut region, instead remaining in the original DiI-labeled position throughout the culture period ($n=5$; Fig. 1H). This finding is in contrast to the contaminated DiI-labeled extraembryonic visceral endoderm which expanded properly into the distal extraembryonic area in the *Sox17*-null embryo (arrowhead in right upper plate of Fig. 1H; Tam et al., 2007). Since *Sox17* activity is cell-autonomously required for hindgut formation (Kanai-Azuma et al., 2002), it provides a useful mouse model for studying potential inductive and supportive functions of hindgut endoderm tissues during the late-headfold to early-somite stages.

PGCs are normally specified and colonized at the base of the allantois in Sox17-null embryos

Next, we examined whether or not PGCs in *Sox17*-null embryos are specified and colonized at the base of the allantois region. At early to late gastrulation stages, several PGCs markers including *Ifitm3/mil-1/fragilis* (Fig. 2A), *Pgc7/Stella/Dppa3*, *Nanog* and *Sox2* (figure not shown) as well as alkaline phosphatase (ALP) activity (Fig. 2B), were properly expressed in *Sox17*-null PGCs, exhibiting similar patterns of expression to those in the wildtype/heterozygote littermates. Moreover, standard whole-mount ALP staining (with all permeabilization procedures) showed that the numbers of ALP-positive PGCs at 7.75 dpc (late-bud to early-headfold stage) were not significantly different between *Sox17*-null and wildtype/heterozygote embryos (Fig. 2C). Sagittal sectioning analyses of some embryos also revealed that PGCs colonized at the base of the allantois and that the front-row population of PGCs moved properly into the PGC entry site of the endoderm layer (arrowheads in Fig. 2D). In the visceral endodermal site proximal to the entrance site (corresponding to the discontinuous and fragmented laminin staining, “white bar” in lower plate of Fig. 2D), a certain population of PGCs was properly found to move close to the visceral endoderm layer in both wildtype and *Sox17*-null embryos (open arrows in Fig. 2D). With regard to proper epigenetic reprogramming and histone modification of PGCs at later stages (described below; see Figs. 4A, B), no appreciable defects in PGCs specification and differentiation in *Sox17*-null mutants were observed, at least until early-somite stages.

Aberrant migration patterns of PGCs in Sox17-null embryos: a small population is immobile within the hindgut entrance while most migrate ectopically toward the extraembryonic endoderm

Spatiotemporal patterns of PGC movement into the outer endoderm layer were examined in *Sox17*-null embryos using whole-mount ALP/HRP double-staining without permeabilization steps. At headfold stage, a small front-row of PGCs moved properly into the PGC entry site at the border of the visceral endoderm region ($n=3$; right in Fig. 3A), showing a similar migratory pattern to that of wildtype embryos at a similar stage (left in Fig. 3A). In wildtype embryos, PGCs in the entrance site increased in number, and then they appear to move into the lateral area of the hindgut region (left in Figs. 3B, C; also see upper plate in Figs. 1D–F). In *Sox17*-null mutant embryos, on the other hand, neither an increase in PGC number nor lateral movement of PGCs in the gut endoderm area occurred (right in Figs. 3B, C). Approximately 10 PGCs appeared to be blocked from moving away from the hindgut entrance site (corresponding to the posterior intestinal portal at later stages) where they remained throughout early organogenic stages (broken rectangles in Figs. 3D–F). This anomaly led to the complete absence of PGCs in the intraembryonic gut region of *Sox17*-null embryos at

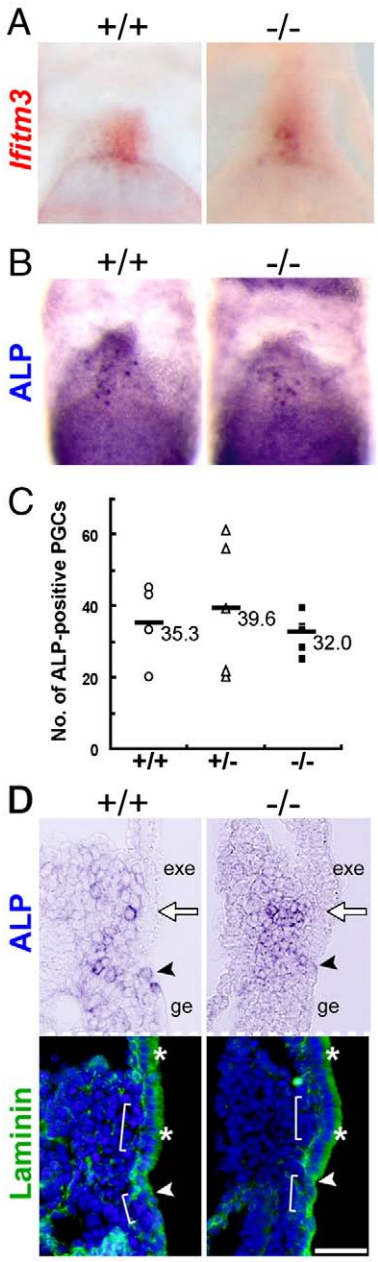

Fig. 2. PGC colonization at the base of the allantois occurs properly in *Sox17*-null embryos at headfold stages. (A) Whole-mount *in situ* hybridization showing *Ifitm3* expression in colonized cells at the base of the allantois in both *Sox17*-null (−/−) and wildtype (+/+) embryos. (B, C) Whole-mount ALP staining showing colonized PGCs (purple in B) and total number of PGCs (C) in wildtype and *Sox17* mutant embryos at headfold stages. No significant differences in PGC number are detectable among wildtype (+/+; open circle), *Sox17*-heterozygote (+/−; open triangle) and *Sox17*-null (−/−; solid rectangle) embryos at 7.75 dpc (early-to-late-headfold stage). In panel C, each value indicates the total PGC number in each embryo, while both bar and number represent the average of the values. (D) ALP (purple staining in upper) and anti-laminin (green fluorescence in lower; DAPI, blue) double-staining of the sagittal sections at the level of the PGC entry site of wildtype (+/+) and *Sox17*-null (−/−) embryos. The front-row PGC population (solid arrowheads in upper) moves properly into the most posterior gut endoderm even in *Sox17*-null embryos. In lower plates, open arrowheads indicate the border between gut endoderm (ge) and extraembryonic visceral endoderm (exe). A certain PGC population appears to be located close to the extraembryonic visceral endoderm (open arrows in upper plates). In the lower plate of D, white bars indicate the area corresponding to the discontinuous and fragmented laminin staining. Asterisks, non-specific staining in visceral endoderm surface. Bar, 50 μm.

later stages (lower right plate in Fig. 3F). Most interestingly, instead of there being no increase in PGC number in the embryonic endoderm area, most PGCs in *Sox17*-null embryos ectopically migrated toward the extraembryonic yolk sac endoderm (arrowheads in Figs. 3B–F). In brief, at early-to-late-headfold stage, *Sox17*-null embryos with four to six PGCs in the endoderm layer showed no ectopic PGCs in the visceral endoderm ($n=3$; inset of Fig. 3A) whereas mutant embryos with more than 10 PGCs in the outer endoderm layer clearly displayed a marked increase in ectopic PGCs in the HRP-positive extraembryonic endoderm area (arrowheads in Figs. 3B–F). The ectopic PGCs in the visceral endoderm appear to be initially located in the visceral endoderm site immediately proximal to the initial PGC entry site containing the front-row (immobile) PGCs (right lower plate in Fig. 3B), and then they migrated away from this site to the extraembryonic endoderm.

To quantitatively examine the number of ectopic PGCs, ALP-positive cells in the gut endoderm, extraembryonic endoderm, and allantois were separately counted in *Sox17*-null and wildtype/heterozygote embryos. While no appreciable change in total PGC number was detected in *Sox17*-null embryos before the 7–8 somite stage, the number was reduced in *Sox17*-null embryos at later stages (Supplementary information, Fig. S2). Even at 8.75 dpc (11–15 somites), a stable population of approximately 10 PGCs was maintained in the hindgut entrance site of *Sox17*-null embryos (solid bars in left graph of Fig. 3G), as opposed to the increase observed in PGCs in the hindgut of the wildtype/heterozygote embryos after 8.5 dpc (open bars in left graph of Fig. 3G). The ectopic PGCs in the extraembryonic endoderm were significantly increased in *Sox17*-null embryos, as compared with those in *Sox17*-wildtype/heterozygote embryos (middle graph of Fig. 3G). However, no significant difference in the number of PGCs in the allantois was observed between wildtype/heterozygote and *Sox17*-null embryos (right graph of Fig. 3G). All these quantitative data support our histological findings showing that, in *Sox17*-null embryos, most of the PGCs except for an immobile PGC population in the hindgut entrance site slipped through the visceral endoderm entrance site and ectopically migrated in an extraembryonic direction during late-headfold to early-somite stages.

Genome-wide epigenetic modification and marker gene expression in ectopic PGCs in the hindgut entrance and extraembryonic endoderm of Sox17-null embryos

Migratory PGCs have previously been shown to undergo a genome-wide dynamic demethylation and histone modification at around the time of entry into the hindgut endoderm (at around 8.0 dpc; Seki et al., 2005, 2007). Using an anti-5-methyl cytosine (MeC) antibody, we examined the genome-wide methylation state of ectopic PGCs located in the hindgut entrance (i.e. posterior intestinal portal) and extraembryonic visceral endoderm in *Sox17*-null embryos (Fig. 4A). In both wildtype and *Sox17*-null embryos at 7.5 dpc (late-bud stage), anti-MeC staining demonstrated fluorescent signals of moderate to high intensity in ALP-positive PGCs at the base of the allantois, similar to those in surrounding extraembryonic mesoderm cells. At 8.5 dpc, signal intensities for anti-MeC staining were reduced in most PGCs located in both the hindgut entrance and extraembryonic endoderm in *Sox17*-null embryos (right in Fig. 4A).

During late-headfold to early-somite stages, it has previously been shown that migratory PGCs reduce histone H3K9 dimethylation at around 8.0 dpc, while they substantially increase the levels of H3K27 trimethylation at around 8.5 dpc (Seki et al., 2005, 2007; left in Fig. 4B). In *Sox17*-null embryos, both PGC populations showed down-regulation of H3K9 dimethylation and up-regulation of H3K27 trimethylation at 8.5 dpc (right in Fig. 4B).

It has been shown that p63, an essential factor in the protection of germ cell lineage during meiotic arrest (Suh et al., 2006), is first activated in migratory PGCs within the hindgut at around 8.5 dpc (Nakamuta and Kobayashi, 2004; left in Fig. 4C). In *Sox17*-null

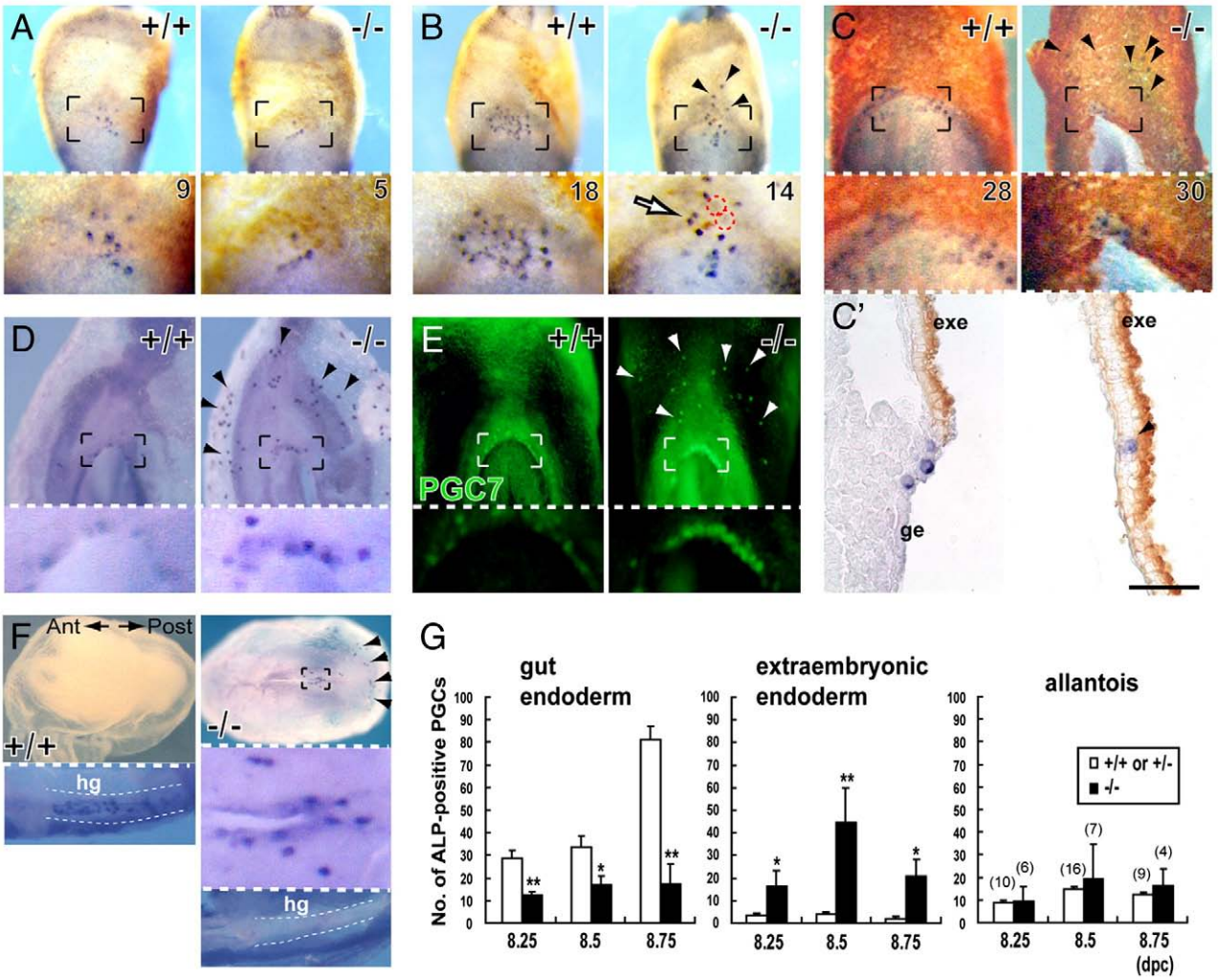

Fig. 3. Aberrant PGC migration in *Sox17*-null embryos. (A–F) Whole-mount ALP (purple staining; A–D [posterior view], F [ventral view]) and anti-PGC7 (green fluorescence; E [posterior view]) staining, showing abnormal PGC migration in *Sox17*-null embryos during early (A)- and late (B)-headfold and early-somite stages (somite number: 2–4 [C], 8–10 [8.5 dpc; D, E], 14–16 [9.0 dpc; F]). Visceral endoderm region is labeled by HRP pre-treatment (brown staining; A–C). In panels A–F, lower plates show the higher magnified images of PGC entry sites in the most posterior gut endoderm region (A–C)/hindgut portals (D–F) indicated by the broken rectangle in the upper plates. The lowest plates in C and F show sagittal sectioning images of posterior region (C′) and ventrolateral views of semi-dissected hindgut tubes (F), respectively. In each embryo of A–C, the number of PGCs which moved out into the endoderm layer is shown in the upper right corner of the lower plate. In *Sox17*-null embryos, a small front-row population of PGCs moves properly into the PGC entry site at the border of the visceral endoderm region (A), but are immobile within this entrance site throughout early embryogenesis (broken rectangles in panels B–F), resulting in a lack of PGCs in the hindgut tube of *Sox17*-null embryos ("hg" in panel F). After the front-row population moves into the hindgut entrance site, most PGCs appear to ectopically slip through the proximal visceral endoderm site (broken red circles [weak ALP-positive PGCs] and open arrow [strong ALP-positive PGCs] in B) and then relocate to the extraembryonic yolk sac endoderm (arrowheads in panels B–F). Bar in panel C, 50 μm. (G) Quantitative analysis showing the numbers of PGCs located in the embryonic gut endoderm (left graph), extraembryonic endoderm (middle) and allantois (right) at 8.25 dpc (1–5 somites), 8.5 dpc (6–10 somites) and 8.75 dpc (11–15 somites) in *Sox17* wildtype/heterozygote ("+/+ or +/−"; open bars), and *Sox17*-null embryos ("−/−"; solid bars). In *Sox17*-null embryos, the PGCs in the gut endoderm are located at the hindgut entrance (solid bars in left graph), while the asterisks on solid bars represent significant differences as compared with those in *Sox17* wildtype/heterozygote embryos at the same stage (single asterisk, $P<0.05$; double asterisk, $P<0.01$). The number in parentheses indicates the number of embryos that were used to count PGCs in each group.

embryos, p63 expression was activated in the nucleus of ectopic PGCs located in both the hindgut entrance and extraembryonic visceral endoderm at 8.5 dpc (right in Fig. 4C). With regard to the quantitative data showing no appreciable reduction in number of ectopic (extraembryonic) PGCs prior to 8.5 dpc (middle graph of Fig. 3G), these data indicate that PGCs undergo epigenetic modifications and differentiation in *Sox17*-null embryos even in the extraembryonic endoderm.

A front-row population of PGCs in the hindgut entrance is tightly surrounded by presumptive endoderm cells in Sox17-null embryos

Since the present DiI-labeling assay shows that *Sox17*-null endoderm displays defective expansion (Fig. 1H), this raises the possibility that the PGCs are trapped by *Sox17*-null definitive endoderm cells incapable of morphogenic movement from the inner mesoderm to the outer endoderm layers. First, we examined the expression patterns of the endoderm marker, E-cadherin, in cells around the hindgut entrance of *Sox17*-null embryos (Figs. 5A–C). In wildtype embryos at headfold stage, E-cadherin is moderately expressed in both embryonic and extraembryonic endoderm cells (Fig. 5B), in addition to a certain E-cadherin-positive population within the extraembryonic allantois (Okamura et al., 2003; asterisk in upper plate of Fig. 5B). Interestingly, in all *Sox17*-null embryos ($n=3$), E-cadherin-positive cells were found to aggregate in the mesodermal region immediately inside the hindgut entrance of the outermost endoderm layer (Fig. 5C), in which several PGCs were tightly surrounded by E-cadherin-positive cells (Fig. 5C′). Ultrastructural analysis also confirmed a close association between PGCs and surrounding endoderm-like cells in

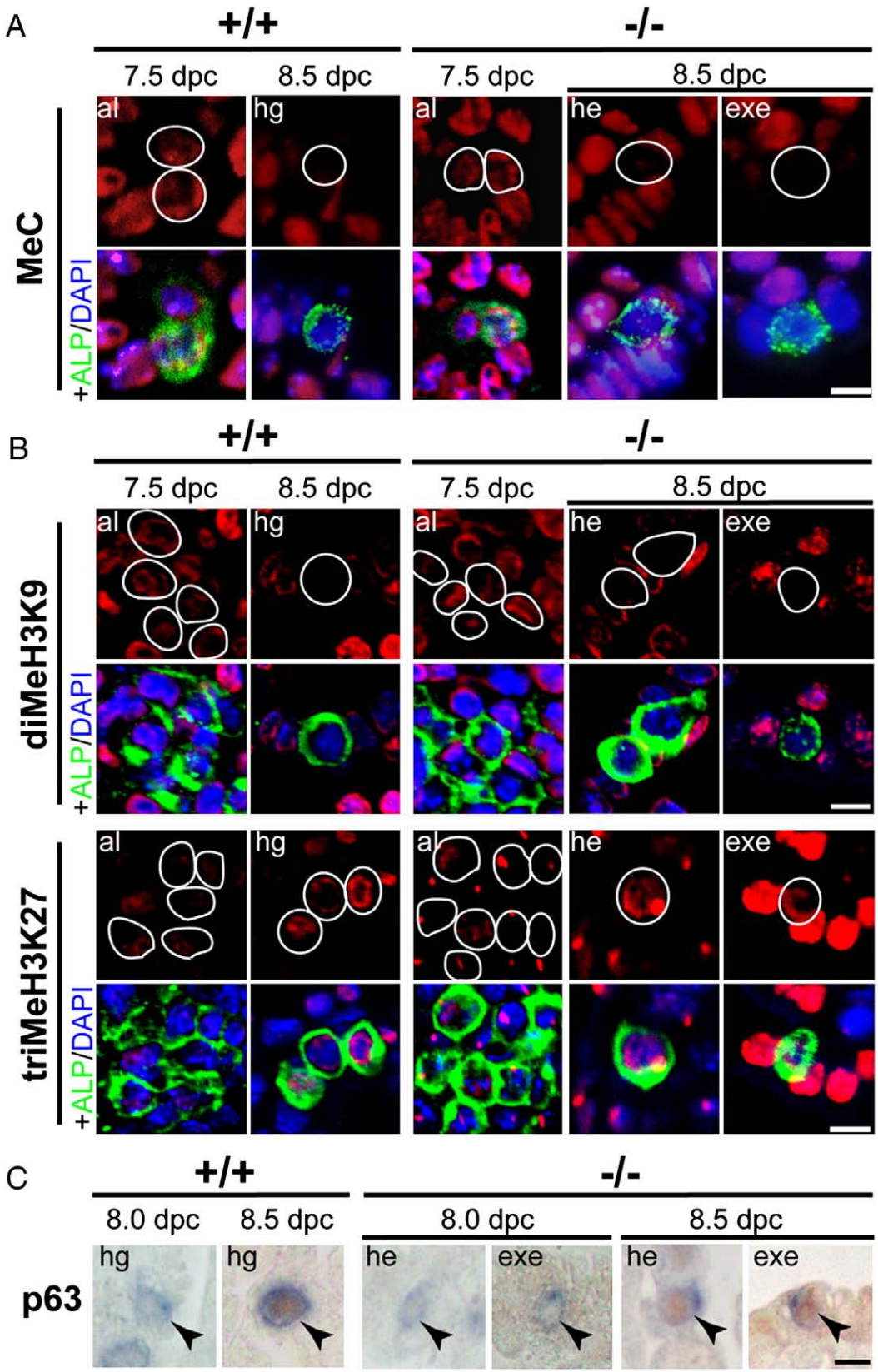

Fig. 4. Genome-wide methylation state, histone modification and marker gene expression in ectopic PGCs of *Sox17*-null embryos. (A, B) Anti-MeC (5-methyl cytosine; (A), anti-diMeH3K9 (dimethyl histone H3K9; upper in panel B) and anti-triMeH3K27 (trimethyl histone H3K27; lower in B) staining (red fluorescence), showing no appreciable defects in the temporal changes of their states in PGCs located in both the hindgut entrance (he) and extraembryonic endoderm (exe) in *Sox17*-null (−/−) embryos. In upper plates, white circles indicate ALP-positive PGCs that are shown in the corresponding lower plates (merged images of ALP [green] and DAPI [blue]). In *Sox17*-null embryos, both populations of PGCs show MeC/diMeH3K9 down-regulation and triMeH3K27 up-regulation from 7.5 to 8.5 dpc, similar to that observed in the hindgut endoderm (hg) of wildtype (+/+) embryos. (C) Anti-p63 (brown staining) and ALP (blue) double-staining showing the proper onset of p63 expression at 8.5 dpc in both PGC populations in the hindgut entrance (he) and extraembryonic endoderm (exe) in *Sox17*-null embryos. al, allantois. Bars, 10 μm.

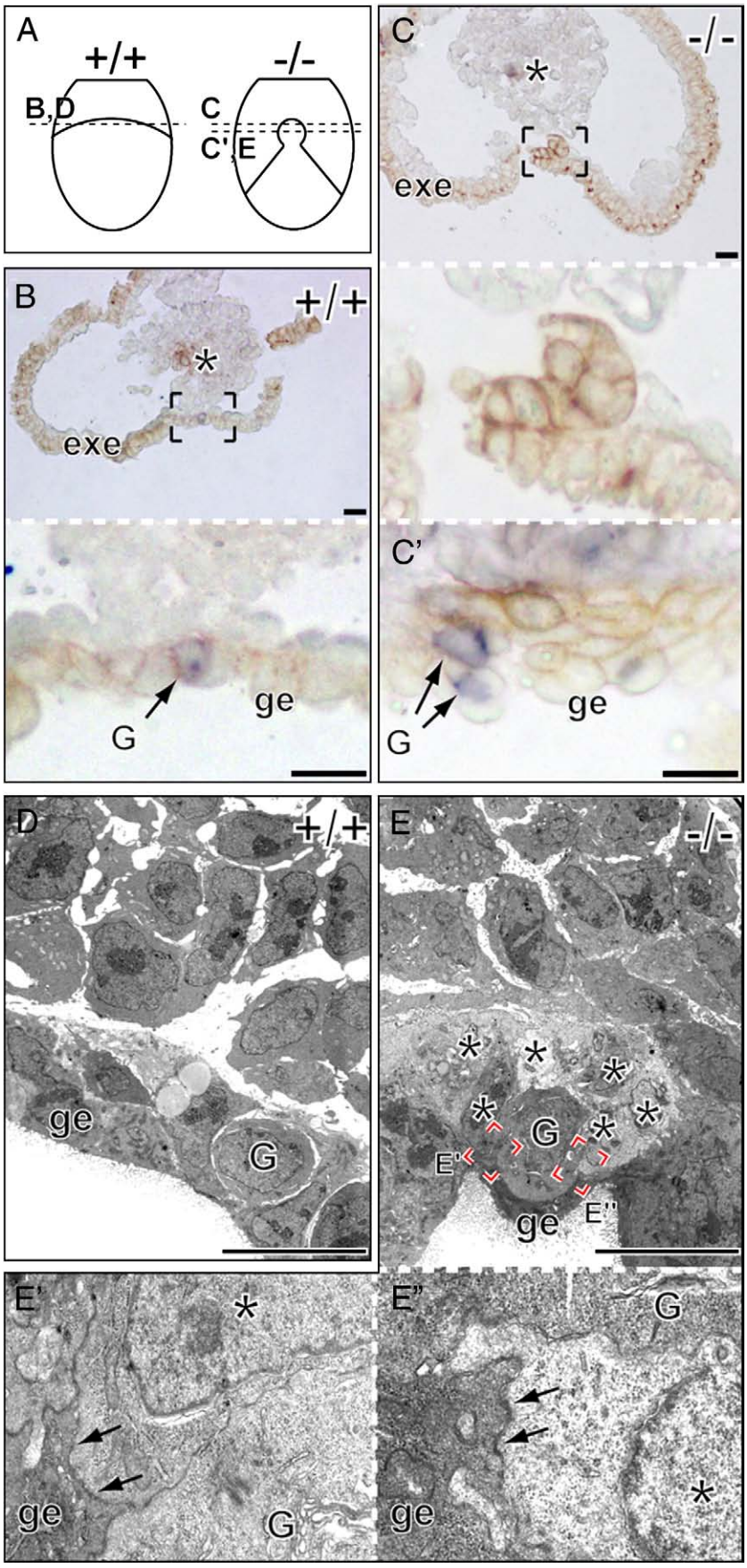
A
+/+
-/-
B,D
C
C'
E
B
+/+
exe
ge
G
C
-/-
exe
C'
ge
G
D
+/+
ge
G
E
-/-
E'
E''
G
ge
E'
ge
G
E''
G
ge

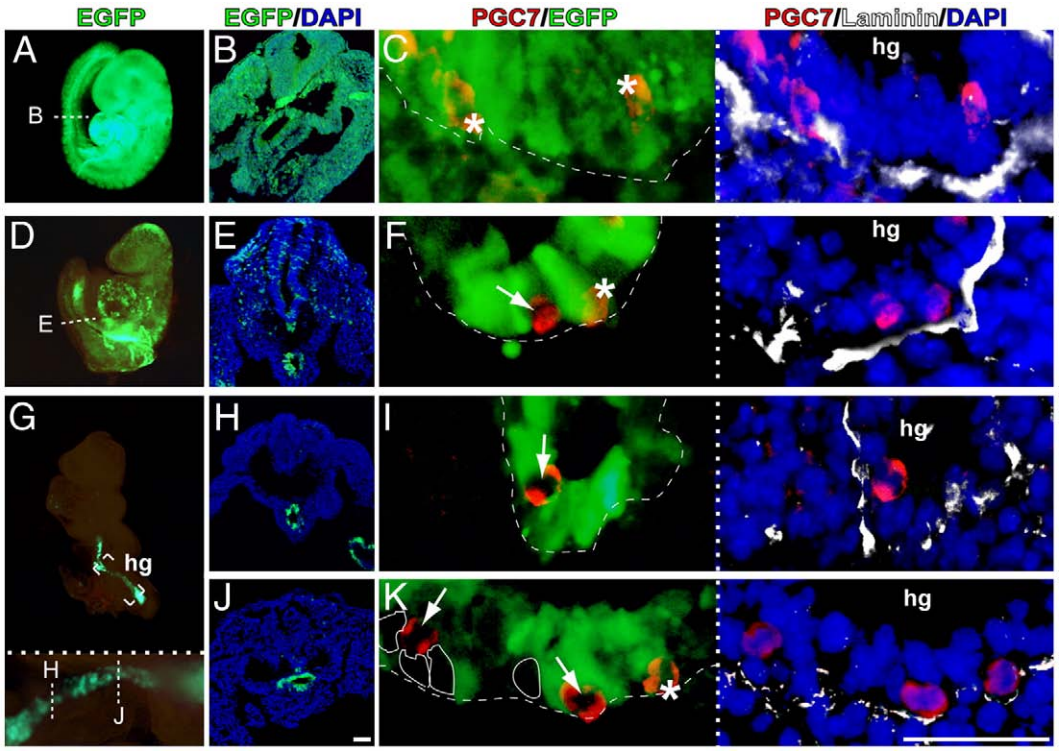

Fig. 6. A supply of *Sox17*$^{+/+}$ endoderm cells can rescue defective PGC migration in *Sox17*-null embryos. Chimeric embryos were generated by blastocyst injection of *Sox17*-null (EGFP-negative) ES cells into EGFP-positive wildtype mice (CAG-EGFP mice). One non-chimeric embryo (A–C), two chimeric embryos (D–F: ~75%; G–K: >95% in mutant ES cell contribution) at around 9.0 dpc (A, D, G: whole-mount images; B, E, H, J: lower magnified sectioning images corresponding to C, F, I and K, respectively). In plates A, D, and G, broken lines indicate the sectioning planes shown in designated plates, while the lower plate in G indicates the higher magnified image of the hindgut (hg) in the upper plate (broken rectangle). In plates C, F, I, and K, anti-PGC7 (red in left)/anti-laminin (white in right) double-staining (EGFP: green in left; DAPI, blue in right) of the same sections, showing that both *Sox17*-null (red; white arrow in left) and *Sox17*$^{+/+}$ (red + green [orange]; white asterisks in left) PGCs properly migrate into and locate in the hindgut walls. In left plates of C, F, I, and K, white broken line indicates the basal border of the gut walls (corresponding to anti-laminin-positive deposition in right plates), while outline circles with a white fine line represent *Sox17*-null endoderm cells. hg, hindgut (in panel G) or lumen of hindgut (in panels C, F, I and K). Bar, 50 μm.

the hindgut entrance of the *Sox17*-null embryo (Figs. 5D, E). These surrounding cells were also found to be tightly connected with neighboring gut endoderm cells located in the outermost layer, where the E-cadherin-based adherens junctions (Nagafuchi, 2001) were widely formed along the cell surface between these two cells (arrows in Figs. 5E′, E″). These data clearly indicate that the E-cadherin-positive cells at the hindgut entrance are presumptive definitive endoderm (or its precursor) cells that are defective in morphogenic movement from the hindgut entrance toward the lateral region of the embryonic gut endoderm. This finding further suggests that such abnormal endoderm cells may trap a front-row population of PGCs, resulting in their sequestration in the entrance point (i.e. posterior intestinal portal) even at later somite stages.

A supply of Sox17$^{+/+}$ *endoderm cells can rescue defective migration of Sox17-null PGCs in chimeric embryos*

To confirm the direct cause of aberrant PGC migration by *Sox17*-null endoderm, we examined PGC behaviors in four high-contribution chimeric embryos (around 8.75–9.0 dpc; >75% EGFP-negative *Sox17*-null cells) consisting of *Sox17*-null ES cells and EGFP-positive *Sox17*$^{+/+}$ blastocysts (Fig. 6). One chimeric embryo with moderate to high mutant ES cell contribution (approximately 75%) was slightly retarded, but morphologically normal (Figs. 6D–F). Three chimeras with a high mutant ES cell contribution (>95%) displayed a reduction in embryonic gut size and failed to undergo axis rotation (Figs. 6G–K), which recapitulates the phenotype of the *Sox17*-null mutant embryos. All these chimeric embryos displayed a marked reduction in the contribution of *Sox17*-null ES cells to hindgut endoderm (Figs. 6D–K), resulting in *Sox17*-null (EGFP-negative) embryos mixed with EGFP-positive *Sox17*$^{+/+}$ gut endoderm cells.

Anti-PGC7/anti-laminin double-staining clearly demonstrated a high contribution of *Sox17*-null ES cells to the PGC lineage in these chimeric embryos (*Sox17*-null PGCs: 272 cells versus wildtype ones: 30 cells; see Table 1). Both *Sox17*-null and *Sox17*$^{+/+}$ PGCs migrated properly to the hindgut tube even in chimeric embryos with reduced gut size (Figs. 6E, F, H–K). In these embryos, EGFP-negative *Sox17*-null PGCs were distributed properly within the EGFP-positive *Sox17*$^{+/+}$ hindgut walls along the AP axis (arrows in Figs. 6F, I, K).

Fig. 5. A front-row PGC population in the hindgut entrance is tightly surrounded by presumptive endoderm cells in *Sox17*-null embryos (3–4 somite stage). (A) Schematic representation showing sectioning planes of plates B–E in wildtype (+/+) and *Sox17*-null (−/−) embryos (posterior views). (B, C) Anti-E-cadherin (brown) and ALP (PGCs; blue) double-staining, showing E-cadherin expression of moderate to high intensity in presumptive endoderm cells at the hindgut entrance in *Sox17*-null embryos (broken rectangle in panel C), in contrast to E-cadherin expression of moderate intensity in definitive endoderm cells of wildtype embryos (B). In upper plates of B and C, asterisks indicate E-cadherin-positive mesenchymal cells at the base of the allantois. (Note the similar signal intensities in both wildtype and *Sox17*-null embryos). Broken rectangles encompass the hindgut entrance magnified in the lower plate. Plate C′ shows anti-E-cadherin staining image of the PGC entry site at the more distal sectioning plane of the same embryos (separated by 2–3 section interval as shown in A). (D, E) Transmission electron micrographs showing PGCs (G) and gut endoderm cells (ge) within the hindgut entrance in wildtype (D) and *Sox17*-null (E) embryos. Red broken rectangles encompass the tight connection images of two inner endoderm-like cells (asterisks) with the outer gut endoderm cell (ge) and PGC (G) as shown in E′ and E″. Adherence-like junctions (arrows) are formed between the outer gut endoderm cell (ge) and the inner presumptive endoderm cells (asterisks). exe, extraembryonic visceral endoderm. Bars, 20 μm.

Table 1
Total cell number of *Sox17*-null/wildtype PGCs in the hindgut and extraembryonic endoderm (exe) in chimeric and non-chimeric embryos at 8.75–9.0 dpc.

Embryo	Location	Genotype		Total PGC number (%)
		Wildtype (+/+) (EGFP-positive)	*Sox17*-null (−/−) (EGFP-negative)	
Non-chimeras (control)	Hindgut	109	–	109 (96)
	exe	4	–	4 (4)
	Total (%)	113	–	113 (100)
High-contribution chimeras	Hindgut	30	265	295 (98)
	exe	0	7	7 (2)
	Total (%)	30 (10)	272 (90)	302 (100)

Sox17-null chimeric embryos mixed with wildtype ($Sox17^{+/+}$) endoderm at 8.75 to 9.0 dpc were generated by blastocyst injection of *Sox17*-null ES cells into C57BL/6-Tg (CAG-EGFP) hosts. The serial cryosections corresponding to the posterior trunk, including the extraembryonic endoderm, were analyzed by anti-PGC7/anti-laminin double-staining of each embryo. The total PGC number in each genotype/each location was counted and pooled in non-chimeric (control, $n=2$) and chimeric (one chimera: ~75%, three chimera: >95% in % in mutant ES cell contribution; $n=4$) embryos.

Since these chimera showed no appreciable increase in ectopic PGCs in yolk sac endoderm as compared with non-chimeric control embryos (Table 1), these findings indicate that abnormal PGC localization is caused by the loss of *Sox17* activity in endoderm cells, not in PGCs themselves.

Discussion

In mouse embryogenesis, the *Sox17* gene is activated in various distinct cell lineages including the definitive endoderm and its derivatives (Kanai-Azuma et al., 2002; Park et al., 2006), visceral endoderm (Kanai-Azuma et al., 2002, Park et al., 2006; Shimoda et al., 2007), vascular endothelial cells (Matsui et al., 2006; Sakamoto et al., 2007), hematopoietic cells (Kim et al., 2007), oligodendrocytes (Sohn et al., 2006) and germ cells (Kanai et al., 1996; Yabuta et al., 2006; de Jong et al., 2008). *Sox17*-null embryos specifically show a reduced population of definitive endoderm cells (i.e., a narrow gut endoderm along the AP axis [Kanai-Azuma et al., 2002]) and defective expansion of hindgut endoderm (this study), but do not display any appreciable defects in other *Sox17*-expressing tissues (Kanai-Azuma et al., 2002; Sakamoto et al., 2007; Shimoda et al., 2007; this study). Such a specific defect in definitive endoderm lineages is likely to be due to the redundancy of other *Sox* members co-expressed in the same cell types (Matsui et al., 2006; Sakamoto et al., 2007; Shimoda et al., 2007; Kurimoto et al., 2008). The present chimera analysis using *Sox17*-null ES cells also enabled us to examine *Sox17*-null embryos mixed with wildtype gut endoderm cells (Kanai-Azuma et al., 2002; Tam et al., 2003; this study). Taken together, these findings indicate that the mouse model using *Sox17*-null/chimeric embryos is very useful in a genetic approach to determining the inductive and supportive roles of gut endoderm in early embryogenesis of mammals.

Using this *Sox17*-null mouse system, the present study provided genetic evidence for a role of hindgut endoderm in the incorporation and displacement of PGC to the embryonic gut domain. In *Sox17*-null embryos, PGCs are specified and localized at the base of the allantois, and then the front-row PGC population (approximately 10 PGCs) moves properly into the hindgut entrance of the most posterior gut endoderm ("green" PGCs in Fig. 7). However, despite the presence of gut endoderm cells in *Sox17*-null embryos, this front-row PGC population is trapped within this restricted hindgut entrance, and migration from this site into the intraembryonic gut endoderm region appears to be blocked. Chimera analysis using *Sox17*-null ES cells demonstrated that this aberrant migration of *Sox17*-null PGCs can be rescued by the supply of wildtype endoderm cells, resulting in normal PGC distribution along the hindgut tube in all chimeric embryos. These data, therefore, indicate that the proper expansion of hindgut endoderm is essential for PGC migration into the intraembryonic gut endoderm in late gastrulation and early somitogenesis. These data clearly provide direct genetic evidence showing a non-cell-autonomous "passive" migration of PGCs at this stage that is directly regulated by hindgut morphogenic movement. This finding is clearly consistent with the previous ultrastructural and time-lapse data showing non-motile morphology (i.e., round shape without pilopodia) of these PGCs in the hindgut (Clark and Eddy, 1975; Anderson et al., 2000; also see Fig. 5D in this study).

Interestingly, the present study revealed that the front-row PGC population was tightly surrounded by E-cadherin-positive endoderm-like cells within the hindgut entrance site of developing *Sox17*-null embryos. Despite the higher level of E-cadherin expression in these endoderm-like cells compared to the gut endoderm of wildtype embryos, these endoderm-like cells were continuously connected with the gut endoderm cells located in the outermost endoderm layer (Fig. 5). It was also shown that, like normal wildtype hindgut cells, these endoderm-like cells have the ability to support PGCs by the early organogenic embryo stage. This is because this immobile PGC population appears to be maintained and to survive even at the later stages (Fig. 3F), which is clearly in contrast to the reduced number of ectopic PGCs in the extraembryonic endoderm. Moreover, the present DiI-labeling assay demonstrated no appreciable lateral morphogenic movement of endoderm-like cells in the entrance site in *Sox17*-null embryos (Fig. 1G). Taken together, these data indicate that, in *Sox17*-null embryos, E-cadherin-positive presumptive endoderm cells aggregate in the hindgut entrance possibly as a cause or consequence of their defective expansion into the outer endoderm layer. As well as wildtype hindgut cells, these cells can catch and support PGCs without morphogenic movement throughout early somitogenesis, resulting in immobile PGCs within the hindgut entrance (i.e. posterior intestinal portal) in *Sox17*-null embryos.

It was previously shown that E-cadherin expression in the PGCs is closely correlated with their migratory activities in various animal species including mice (Bendel-Stenzel et al., 2000; Di Carlo and De Felici, 2000; Blaser et al., 2005; Kunwar et al., 2008). Although we could not estimate its expression in the PGCs within the gut endoderm, it is also likely that E-cadherin expression in gut endoderm cells affects the morphogenic expansion of gut endoderm cells in mouse gastrulation (Burtscher and Lickert, 2009). Interestingly, in contrast to an aberrant high level of E-cadherin expression in the presumptive hindgut endoderm cells of the *Sox17-null* embryos (Fig. 5C), our preliminary experiments revealed that no appreciable differences in E-cadherin expression levels were detected between *Sox17*-null and wildtype hindgut endoderm cells in the high-contribution chimeric embryo (see Supplementary information, Fig. S3). These data imply that an aberrant high level of E-cadherin expression in *Sox17*-null endoderm cells can be rescued by the supply of the wildtype endoderm cells, indicating a close correlation between aberrant E-cadherin expression and defective morphogenic expansion in *Sox17*-null hindgut endoderm cells. Further analyses are required to clarify the *Sox17*-downstream non-cell autonomous mechanisms involved in the proper regulation of E-cadherin expression levels in hindgut endoderm cells during late gastrulation.

As described above, the present study demonstrates a "passive" PGC migration from the entrance site of the most posterior gut endoderm into the lateral gut area at late-headfold to early-somite stages. This study also demonstrated that the front-row PGC population can properly move and reach the presumptive endoderm area (corresponding to posterior intestinal portal) even in *Sox17*-null embryos without hindgut movement. Moreover, it was shown that, in this mutant, most of the remaining PGCs (approximately 20 cells) slip through the visceral endoderm entrance site, and then migrate toward the ectopic yolk sac endoderm during late gastrulation ("blue" PGCs in Fig. 7). These findings suggest that the PGC movement from the allantois mesoderm into the outer endoderm layer occurs properly in *Sox17*-null embryos. This in turn indicates no appreciable contribution

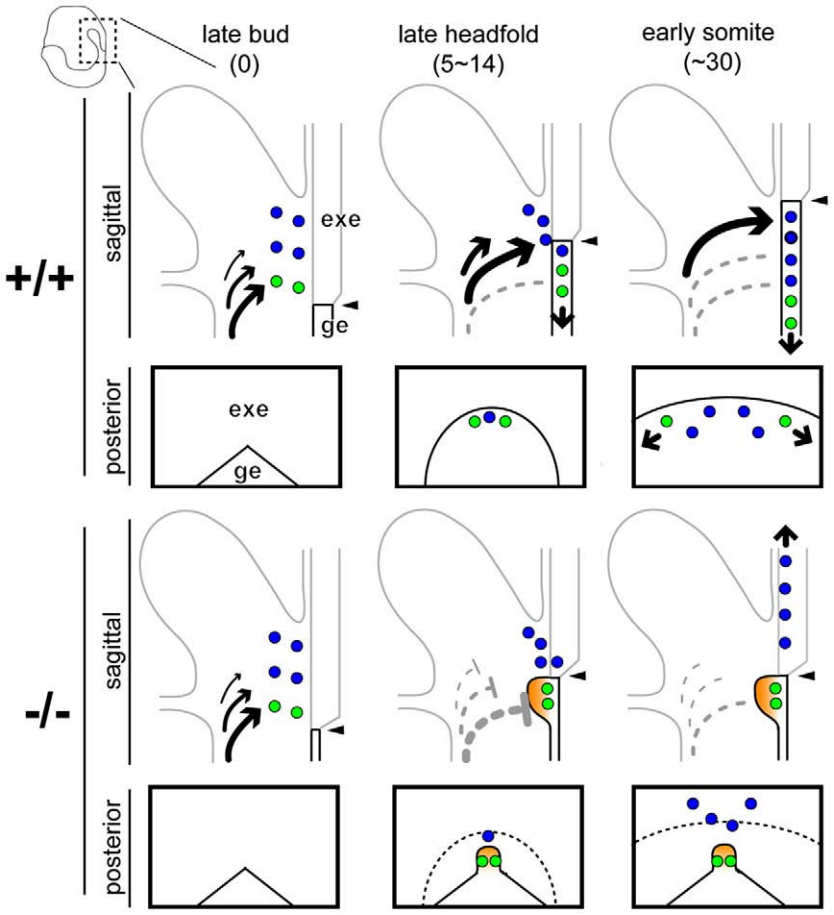

Fig. 7. Schematic representation showing spatiotemporal patterns of PGC migration from extraembryonic allantois mesoderm into intraembryonic endoderm in wildtype and *Sox17*-null embryos. Schematic representation (upper, sagittal sectioning views; lower, posterior views), showing spatiotemporal patterns of PGC migration (round cells) and hindgut morphogenic movement (bold arrows) in the hindgut entrance site of wildtype (+/+, upper) and *Sox17*-null (−/−, lower) embryos. In wildtype embryos, the PGCs appear to move from the allantois into the outer endoderm layer at the exact same time as the distal-to-proximal wave pattern of hindgut morphogenic movement. They are then non-cell-autonomously transferred from the hindgut entrance into the intraembryonic gut region possibly in a conveyor belt-type manner. In *Sox17*-null embryos, PGCs are normally specified and colonized in the allantois, and then the front-row PGC population moves properly into the hindgut entrance at the most posterior gut endoderm ("green" PGCs). However, due to defective hindgut expansion into the gut endoderm layer (gray dashed line), E-cadherin-positive endoderm cells aggregate and catch the front-row PGC population in the hindgut entrance ("orange" area), leading to the failure of PGC spreading toward the intraembryonic gut endoderm in *Sox17*-null embryos. At the same time, most of the remaining PGCs slip through the visceral endoderm entrance site and ectopically migrate toward the ectopic yolk sac endoderm ("blue" PGCs). exe, extraembryonic visceral endoderm; ge, gut endoderm.

of hindgut morphogenic movement to PGC transport from the allantois mesoderm into the endoderm, further suggesting an "active" PGC migration from the mesoderm into the endoderm at late gastrulation stages (Anderson et al., 2000).

The formation of germ layers requires the dynamic movement of progenitor cells from the epiblast through the primitive streak, either emerging as a new mesoderm layer or becoming incorporated as definitive endoderm into the pre-existing visceral endoderm layer (Tam and Loebel, 2007). Recently, Kwon et al. (2008) reported that gut endoderm formation occurs by dynamic widespread intercalation of definitive endoderm and visceral endoderm lineages. They demonstrated that visceral endoderm cells positively contribute to the formation of parts of the gut endoderm region, especially the hindgut tube, in late gastrulation. In *Sox17*-null mutants, the majority of PGCs slip through the visceral endoderm entrance site toward the ectopic yolk sac endoderm, while the supply of wildtype endoderm restores the lateral migration of these PGCs from the visceral endoderm into the gut endoderm. Therefore, it is likely that the defective supply and expansion of definitive endoderm cells in *Sox17*-null mutants prevent the incorporation of visceral endoderm cells containing PGCs into the intraembryonic gut endoderm, resulting in ectopic PGCs remaining in the extraembryonic region. This in turn suggests that, in wildtype embryos, the dynamic morphogenic movement of hindgut precursor cells coincides precisely with PGC migration into the outer visceral endoderm layer. Following this, the differentiating hindgut cells appear to take hold of the PGCs just beneath the entrance site of the most posterior gut endoderm and to transfer them to the intraembryonic gut region possibly in a conveyor belt-type manner.

To date, a close association of morphogenic movement of gut endoderm with migratory PGCs has also been reported in various animal species including *Drosophila* and *C. elegans*, despite the anatomical differences among the embryos. In *Drosophila*, it has been shown that PGCs are incorporated into the posterior midgut morphogenesis (Warrior, 1994). In *C. elegans*, germ cell (P_4) follows the neighboring two gut endodermal cells (E) in the ingression of cells during gastrulation (Sulston et al., 1983; Powell-Coffman et al., 1996). Therefore, the morphogenic gastrulation movement of the gut endoderm plays a conserved, crucial role in PGC transport into the intraembryonic area within the receiving range of guidance cues from genital ridges such as SDF-1 and Steel (Buehr et al., 1993; Ara et al., 2003; Molyneaux et al., 2003; Runyan et al., 2006). The present study also highlighted the importance of the spatiotemporal synchronized movement of PGCs and hindgut cells in the most posterior gut endoderm during late gastrulation. This provides definite impetus for further studies to clarify molecular mechanisms underlying the synchronous regulation of the following two independent events in mouse late gastrulation: (1) the PGC transition from mesoderm to

endoderm layer, and (2) the morphogenic movement of hindgut progenitor cells.

Acknowledgments

The authors wish to thank Prof. Dr. Patrick Tam for his kind critical reading and comments on the manuscript. The authors also wish to thank Dr. Satomi Tanaka for his kind critical reading and providing the *Ifitm3 in situ* probe. The authors also thank Prof. Dr. Yasuhisa Matsui for providing the PGC7 antibody. The authors wish to thank Miss. Rie Ishii and Mr. Minoru Fukuda for their technical assistance, and Ms. Itsuko Yagihashi for her secretarial assistance. This work was supported by financial grants from the Ministry of Education, Science, Sports and Culture of Japan (Y.K.). K.H. is a DC1 JSPS Research Fellow.

Appendix A. Supplementary data

Supplementary data associated with this article can be found, in the online version, at doi:10.1016/j.ydbio.2009.04.012.

References

Alexander, J., Stainier, D.Y., 1999. A molecular pathway leading to endoderm formation in zebrafish. Curr. Biol. 9, 1147–1157.
Anderson, R., Copeland, T.K., Schöler, H., Heasman, J., Wylie, C., 2000. The onset of germ cell migration in the mouse embryo. Mech. Dev. 91, 61–68.
Ara, T., Nakamura, Y., Egawa, T., Sugiyama, T., Abe, K., Kishimoto, T., Matsui, Y., Nagasawa, T., 2003. Impaired colonization of the gonads by primordial germ cells in mice lacking a chemokine, stromal cell-derived factor-1 (SDF-1). Proc. Natl. Acad. Sci. U. S. A. 100, 5319–5323.
Bendel-Stenzel, M.R., Gomperts, M., Anderson, R., Heasman, J., Wylie, C., 2000. The role of cadherins during primordial germ cell migration and early gonad formation in the mouse. Mech. Dev. 91, 143–152.
Bielinska, M., Narita, N., Wilson, D.B., 1999. Distinct roles for visceral endoderm during embryonic mouse development. Int. J. Dev. Biol. 43, 183–205.
Blaser, H., Eisenbeiss, S., Neumann, M., Reichman-Fried, M., Thisse, B., Thisse, C., Raz, E., 2005. Transition from non-motile behaviour to directed migration during early PGC development in zebrafish. J. Cell. Sci. 118, 4027–4038.
Boldajipour, B., Mahabaleshwar, H., Kardash, E., Reichman-Fried, M., Blaser, H., Minina, S., Wilson, D., Xu, Q., Raz, E., 2008. Control of chemokine-guided cell migration by ligand sequestration. Cell 132, 463–473.
Buehr, M., McLaren, A., Bartley, A., Darling, S., 1993. Proliferation and migration of primordial germ cells in We/We mouse embryos. Dev. Dyn. 198, 182–189.
Burtscher, I., Lickert, H., 2009. Foxa2 regulates polarity and epithelialization in the endoderm germ layer of the mouse embryo. Development 136, 1029–1038.
Clark, J.M., Eddy, E.M., 1975. Fine structural observations on the origin and associations of primordial germ cells of the mouse. Dev. Biol. 47, 136–155.
de Jong, J., Stoop, H., Gillis, A.J., van Gurp, R.J., van de Geijn, G.J., Boer, M., Hersmus, R., Saunders, P.T., Anderson, R.A., Oosterhuis, J.W., Looijenga, L.H., 2008. Differential expression of SOX17 and SOX2 in germ cells and stem cells has biological and clinical implications. J. Pathol. 215, 21–30.
de Napoles, M., Nesterova, T., Brockdorff, N., 2007. Early loss of Xist RNA expression and inactive X chromosome associated chromatin modification in developing primordial germ cells. PLoS ONE 2, e860.
Di Carlo, A., De Felici, M., 2000. A role for E-cadherin in mouse primordial germ cell development. Dev. Biol. 226, 209–219.
Doitsidou, M., Reichman-Fried, M., Stebler, J., Köprunner, M., Dörries, J., Meyer, D., Esguerra, C.V., Leung, T., Raz, E., 2002. Guidance of primordial germ cell migration by the chemokine SDF-1. Cell 111, 647–659.
Herpin, A., Fischer, P., Liedtke, D., Kluever, N., Neuner, C., Raz, E., Schartl, M., 2008. Sequential SDF1a and b-induced mobility guides Medaka PGC migration. Dev. Biol. 320, 319–327.
Hudson, C., Clements, D., Friday, R.V., Stott, D., Woodland, H.R., 1997. Xsox17alpha and -beta mediate endoderm formation in *Xenopus*. Cell 91, 397–405.
Kanai, Y., Kanai-Azuma, M., Noce, T., Saido, T.C., Shiroishi, T., Hayashi, Y., Yazaki, K., 1996. Identification of two Sox17 messenger RNA isoforms, with and without the high mobility group box region, and their differential expression in mouse spermatogenesis. J. Cell Biol. 133, 667–681.
Kanai-Azuma, M., Kanai, Y., Okamoto, M., Hayashi, Y., Yonekawa, H., Yazaki, K., 1999. Nrk: a murine X-linked NIK (Nck-interacting kinase)-related kinase gene expressed in skeletal muscle. Mech. Dev. 89, 155–159.
Kanai-Azuma, M., Kanai, Y., Gad, JM., Tajima, Y., Taya, C., Kurohmaru, M., Sanai, Y., Yonekawa, H., Yazaki, K., Tam, PP., Hayashi, Y., 2002. Depletion of definitive gut endoderm in *Sox17*-null mutant mice. Development 129, 2367–2379.
Kim, I., Saunders, T.L., Morrison, S.J., 2007. Sox17 dependence distinguishes the transcriptional regulation of fetal from adult hematopoietic stem cells. Cell 130, 470–483.
Knaut, H., Werz, C., Geisler, R., Nüsslein-Volhard, C., Tübingen 2000 Screen Consortium, 2003. A zebrafish homologue of the chemokine receptor Cxcr4 is a germ-cell guidance receptor. Nature 421, 279–282.
Kunwar, P.S., Sano, H., Renault, A.D., Barbosa, V., Fuse, N., Lehmann, R., 2008. Tre1 GPCR initiates germ cell transepithelial migration by regulating *Drosophila melanogaster* E-cadherin. J. Cell Biol. 183, 157–168.
Kurimoto, K., Yabuta, Y., Ohinata, Y., Shigeta, M., Yamanaka, K., Saitou, M., 2008. Complex genome-wide transcription dynamics orchestrated by Blimp1 for the specification of the germ cell lineage in mice. Genes Dev. 22, 1617–1635.
Kwon, G.S., Viotti, M., Hadjantonakis, A.K., 2008. The endoderm of the mouse embryo arises by dynamic widespread intercalation of embryonic and extraembryonic lineages. Dev. Cell 15, 509–520.
Lange, U.C., Adams, D.J., Lee, C., Barton, S., Schneider, R., Bradley, A., Surani, M.A., 2008. Normal germ line establishment in mice carrying a deletion of the Ifitm/Fragilis gene family cluster. Mol. Cell Biol. 28, 4688–4696.
Matsui, T., Kanai-Azuma, M., Hara, K., Matoba, S., Hiramatsu, R., Kawakami, H., Kurohmaru, M., Koopman, P., Kanai, Y., 2006. Redundant roles of Sox17 and Sox18 in postnatal angiogenesis in mice. J. Cell Sci. 119, 3513–3526.
McLaren, A., Lawson, K.A., 2005. How is the mouse germ-cell lineage established? Differentiation 73, 435–437.
Molyneaux, K., Wylie, C., 2004. Primordial germ cell migration. Int. J. Dev. Biol. 48, 537–544.
Molyneaux, K.A., Zinszner, H., Kunwar, P.S., Schaible, K., Stebler, J., Sunshine, M.J., O'Brien, W., Raz, E., Littman, D., Wylie, C., Lehmann, R., 2003. The chemokine SDF1/CXCL12 and its receptor CXCR4 regulate mouse germ cell migration and survival. Development 130, 4279–4286.
Nagafuchi, A., 2001. Molecular architecture of adherens junctions. Curr. Opin. Cell Biol. 13, 600–603.
Nakamuta, N., Kobayashi, S., 2004. Expression of p63 in the mouse primordial germ cells. J. Vet. Med. Sci. 66, 1365–1370.
Nishiumi, F, Komiya, T, Ikenishi, K., 2005. The mode and molecular mechanisms of the migration of presumptive PGC in the endoderm cell mass of *Xenopus* embryos. Dev. Growth Differ. 47, 37–48.
Ohinata, Y., Payer, B., O'Carroll, D., Ancelin, K., Ono, Y., Sano, M., Barton, S.C., Obukhanych, T., Nussenzweig, M., Tarakhovsky, A., Saitou, M., Surani, M.A., 2005. Blimp1 is a critical determinant of the germ cell lineage in mice. Nature 436, 207–213.
Okamura, D., Kimura, T., Nakano, T., Matsui, Y., 2003. Cadherin-mediated cell interaction regulates germ cell determination in mice. Development 130, 6423–6430.
Park, K.S., Wells, J.M., Zorn, A.M., Wert, S.E., Whitsett, J.A., 2006. Sox17 influences the differentiation of respiratory epithelial cells. Dev. Biol. 294, 192–202.
Powell-Coffman, J.A., Knight, J., Wood, W.B., 1996. Onset of *C. elegans* gastrulation is blocked by inhibition of embryonic transcription with an RNA polymerase antisense RNA. Dev. Biol. 178, 472–483.
Runyan, C., Schaible, K., Molyneaux, K., Wang, Z., Levin, L., Wylie, C., 2006. Steel factor controls midline cell death of primordial germ cells and is essential for their normal proliferation and migration. Development 133, 4861–4869.
Sakamoto, Y., Hara, K., Kanai-Azuma, M., Matsui, T., Miura, Y., Tsunekawa, N., Kurohmaru, M., Saijoh, Y., Koopman, P., Kanai, Y., 2007. Redundant roles of Sox17 and Sox18 in early cardiovascular development of mouse embryos. Biochem. Biophys. Res. Commun. 360, 539–544.
Sasado, T., Yasuoka, A., Abe, K., Mitani, H., Furutani-Seiki, M., Tanaka, M., Kondoh, H., 2008. Distinct contributions of CXCR4b and CXCR7/RDC1 receptor systems in regulation of PGC migration revealed by medaka mutants kazura and yanagi. Dev. Biol. 320, 328–339.
Sasaki, H., Matsui, Y., 2008. Epigenetic events in mammalian germ-cell development: reprogramming and beyond. Nat. Rev., Genet. 9, 129–140.
Seki, Y., Hayashi, K., Itoh, K., Mizugaki, M., Saitou, M., Matsui, Y., 2005. Extensive and orderly reprogramming of genome-wide chromatin modifications associated with specification and early development of germ cells in mice. Dev. Biol. 278, 440–458.
Seki, Y., Yamaji, M., Yabuta, Y., Sano, M., Shigeta, M., Matsui, Y., Saga, Y., Tachibana, M., Shinkai, Y., Saitou, M., 2007. Cellular dynamics associated with the genome-wide epigenetic reprogramming in migrating primordial germ cells in mice. Development 134, 2627–2638.
Shimoda, M., Kanai-Azuma, M., Hara, K., Miyazaki, S., Kanai, Y., Monden, M., Miyazaki, J., 2007. Sox17 plays a substantial role in late-stage differentiation of the extraembryonic endoderm in vitro. J. Cell Sci. 120, 3859–3869.
Sohn, J., Natale, J., Chew, L.J., Belachew, S., Cheng, Y., Aguirre, A., Lytle, J., Nait-Oumesmar, B., Kerninon, C., Kanai-Azuma, M., Kanai, Y., Gallo, V., 2006. Identification of Sox17 as a transcription factor that regulates oligodendrocyte development. J. Neurosci. 26, 9722–9735.
Stebler, J., Spieler, D., Slanchev, K., Molyneaux, K.A., Richter, U., Cojocaru, V., Tarabykin, V., Wylie, C., Kessel, M., Raz, E., 2004. Primordial germ cell migration in the chick and mouse embryo: the role of the chemokine SDF-1/CXCL12. Dev. Biol. 272, 351–361.
Sturm, K., Tam, P.P., 1993. Isolation and culture of whole postimplantation embryos and germ layer derivatives. Methods Enzymol. 225, 164–190.
Subtelny, S., Penkala, J.E., 1984. Experimental evidence for a morphogenetic role in the emergence of primordial germ cells from the endoderm in *Rana pipiens*. Differentiation 26, 211–219.
Sugimoto, M., Abe, K., 2007. X chromosome reactivation initiates in nascent primordial germ cells in mice. PLoS Genet. 3, e116.
Suh, E.K., Yang, A., Kettenbach, A., Bamberger, C., Michaelis, A.H., Zhu, Z., Elvin, J.A., Bronson, R.T., Crum, C.P., McKeon, F., 2006. p63 protects the female germ line during meiotic arrest. Nature 444, 624–628.
Sulston, J.E., Schierenberg, E., White, J.G., Thomson, J.N., 1983. The embryonic cell lineage of the nematode *Caenorhabditis elegans*. Dev. Biol. 100, 64–119.
Tam, P.P., Loebel, D.A., 2007. Gene function in mouse embryogenesis: get set for gastrulation. Nat. Rev., Genet. 8, 368–381.

Tam, P.P., Kanai-Azuma, M., Kanai, Y., 2003. Early endoderm development in vertebrates: lineage differentiation and morphogenetic function. Curr. Opin. Genet. Dev. 13, 393–400.
Tam, P.P., Khoo, P.L., Lewis, S.L., Bildsoe, H., Wong, N., Tsang, T.E., Gad, J.M., Robb, L., 2007. Sequential allocation and global pattern of movement of the definitive endoderm in the mouse embryo during gastrulation. Development 134, 251–260.
Tanaka, S.S., Matsui, Y., 2002. Developmentally regulated expression of mil-1 and mil-2, mouse interferon-induced transmembrane protein like genes, during formation and differentiation of primordial germ cells. Mech. Dev. 119 (Suppl. 1), S261–S267.
Tanaka, S.S., Yamaguchi, Y.L., Tsoi, B., Lickert, H., Tam, P.P., 2005. IFITM/Mil/fragilis family proteins IFITM1 and IFITM3 play distinct roles in mouse primordial germ cell homing and repulsion. Dev. Cell 9, 745–756.
Warrior, R., 1994. Primordial germ cell migration and the assembly of the *Drosophila* embryonic gonad. Dev. Biol. 166, 180–194.
Whitington, P.M., Dixon, K.E., 1975. Quantitative studies of germ plasm and germ cells during early embryogenesis of *Xenopus laevis*. J. Embryol. Exp. Morphol. 33, 57–74.
Yabuta, Y., Kurimoto, K., Ohinata, Y., Seki, Y., Saitou, M., 2006. Gene expression dynamics during germline specification in mice identified by quantitative single-cell gene expression profiling. Biol. Reprod. 75, 705–716.